MAPPING VERTICAL LAND MOVEMENT IN SINGAPORE USING INSAR AND GPS

J. Catalão [(1)], D. Raju [(2)], R.M.S. Fernandes [(3)]

[(1)] Universidade de Lisboa, IDL, Lisboa, Portugal (jcfernandes@fc.ul.pt)
[(2)] Tropical Marine Science Institute, National University of Singapore, Singapore.
[(3)] Universidade Beira Interior, IDL, Covilhã, Portugal.

ABSTRACT

In this study we investigate the spatial variation in vertical land motion (VLM) along the coast of Singapore over the past two decades and we examine the impact of spatially variable VLM on relative sea level trends. For that, we use an integrated approach based on the merging of terrain displacement velocities estimated by time series of interferometric synthetic aperture radar (InSAR) data acquired along ascending and descending orbits and repeated GPS measurements.
We processed 39 single look complex images from ERS2 satellite (ascending and descending passes) spanning from October 1995 until January 2000. The vertical velocities of 5 continuous GPS stations of the Singapore Satellite Positioning Reference Network (SiReNT) were used as constraints in the PS solutions to further enhance the solution quality.
The results show that Singapore mainland has experienced subsidence phenomena from 1995 to 2000 with a mean subsidence rate of -1.5 mm/yr. On some localized areas, a significant subsidence with rates of -7 mm/yr was detected. Highest subsiding rates are near the shore on low flat land, above 5m, associated with reclaimed areas or built areas in the past years. The result seems to be reliable and consistent with the geologic setting. The scatter pattern of the deformation indicates anthropogenic causes, related with compaction of built and/or reclaimed areas, rather than natural causes.

1. INTRODUCTION

Global mean sea level rise associated with global warming has a major impact on coastal areas and represents one of the significant natural hazards. The Asia-Pacific region, which has the highest concentration of human population in the world, represents one of the larger areas on Earth being threatened by the rise of sea level. Recent studies indicate a global sea level of 3.2mm/yr measured from 20 years of satellite altimetry [1]. Combined effect of sea level rise with local land subsidence, can be overwhelming for coastal areas. Singapore has undergone relative subsidence which created many small islands. Submergence also accelerates coastal erosion because it facilitates greater inland penetration of storm waves e.g. the observed accelerated erosion in East Coast of Singapore, a reclaimed land area with 185 hectares [2].

The movement of ground can be attributed to natural processes or to human activity – and such movements can often be sufficient to cause coastal hazards and risk to coastal infrastructure. These ground movements are traditionally monitored on-site with traditional geodetic instruments and with GNSS. In recent years, repeat-pass space-borne Synthetic Aperture Radar Interferometry, (InSAR) has been also applied to monitor ground subsidence in urban areas, mostly related to the construction of important engineering structures [3],[4],[5].

In this study we used InSAR Persistent Scatterers technique to determine the spatial variation in vertical land motion (VLM) along the coast of the Singapore over the past decade, and to combine PS results with cGPS (continuous GPS) observations, to examine the impact of spatially variable VLM on relative sea level trends. Our approach will take advantage of the synergistic aspects of these techniques, GPS providing long-term stability, good resolution of horizontal motions and broad scale control on rates and patterns of deformation and InSAR providing high spatial resolution and high sensitivity to vertical motions.

2. SAR DATA

A set of 23+16 images from satellites ERS1 and ERS2 was obtained from the European Space Agency (ESA) under contract CAT1-6940 (Project "Mapping Vertical Land Movement and Coastline Retreat Study Using InSAR and GNSS"). The images were acquired along ascending (track 226) and descending (track 75) passes and covers the period 1995-2000 (Tab. 1). A master date was chosen for each track based on the minimization of the perpendicular baseline and temporal baseline. The master for track 75 is the image acquired on 1997, September 7 and for the track 226 the image acquired on 1997, November 27. The resulting time series of perpendicular and temporal baselines are also shown on Tab. 1. In principle, the higher the baseline the more accurate the altitude measurement, since the phase noise is equivalent to a smaller altitude noise. However, the progressive increase of the baseline and therefore the progressive change in viewing angle implies that the fringe frequency increases to be finally greater than the signal bandwidth thus making the fringe

Proc. 'ESA Living Planet Symposium 2013', Edinburgh, UK
9–13 September 2013 (ESA SP-722, December 2013)

not observable. Larger baselines thus produce fringes with increasing frequency. Hence, there is an optimum perpendicular baseline that maximises the signal to noise power ratio (where the signal is terrain altitude). In the ERS case, such an optimum baseline is about 300–400 metres [6]. For the descending pass most of the acquisitions have perpendicular baselines out of the optimal baseline limit and some are out of the outmost limit (around 800m). Besides, the images are unevenly distributed with some time gaps of more than 200 days, about 7 cycles. The consequences of both effects are the degradation of the coherence. The changes with time of the scattering properties of the target reduce the coherence, which also decreases linearly with the increase of the baseline, thus increasing the phase noise. For the ascending pass, the perpendicular baselines are within the optimal baseline limit but the SAR data time series has a time gap of more than one year. Also the number of acquisitions is not enough to properly model the atmospheric effects. Colesanti et al., [7], suggests a minimum number of 25-30 interferograms to properly identify the PSs and around 3-4 Ps/km^2 to properly estimate and remove the atmospheric phase screen.

Table 1: *ERS1 and ERS2 SAR data.*

Descending pass (trk75)			Ascending pass (trk226)		
Date	$B_\perp$	B_T	Date	$B_\perp$	B_T
07-Oct-1995	525	-701	09-Apr-1996	-382	-596
31-Mar-1996	-490	-525	10-Apr-1996	-288	-595
04-May-1996	997	-491	14-May-1996	-451	-561
05-May-1996	859	-490	15-May-1996	-286	-560
18-Aug-1996	-886	-385	09-Jul-1997	268	-140
22-Sep-1996	-35	-350	17-Sep-1997	388	-70
27-Oct-1996	839	-315	22-Oct-1997	202	-35
01-Dec-1996	352	-280	26-Nov-1997	0	0
03-Aug-1997	-236	-35	31-Dec-1997	-321	35
07-Sep-1997	0	0	11-Mar-1998	299	105
11-Oct-1997	170	34	20-May-1998	217	175
12-Oct-1997	513	35	24-Jun-1998	441	210
16-Nov-1997	-233	70	29-Jul-1998	-225	245
01-Mar-1998	-920	175	02-Sep-1998	-334	280
23-Aug-1998	-348	350	07-Oct-1998	-423	315
27-Sep-1998	464	385	16-Dec-1998	338	385
01-Nov-1998	493	420			
10-Jan-1999	-1213	490			
21-Mar-1999	338	560			
30-May-1999	669	630			
08-Aug-1999	376	700			
17-Oct-1999	-392	770			
30-Jan-2000	-220	875			

3. SAR INTERFEROMETRIC PROCESSING

The interferometric dataset was processed by choosing one master for descending pass (1997, Sep. 7), and one master for the ascending pass (1997, Nov. 26) The master date was chosen minimizing both the temporal and the perpendicular baselines.

Interferograms were computed using the DORIS software [8], with a 1x5 multi-looking and a spatial resolution of 20x20m. Azimuth filtering was applied to all SAR images reducing the noise in the interferometric phase if the master and slave image have a different Doppler centroid frequency. Precise orbits from ESA and Delft was used to compute the geometric shift between the two images. Also baseline information is obtained in this step and written to the result file. DORIS software has implemented a coregistration procedure based on DTM and on the precise orbit data. We did not use the DTM procedure due to the lower heights of Singapore. The offset of the slave with respect to the master is determined using a grid of tie points were a cross-correlation of the amplitude patches is performed. Using this information a coregistration polynomial is determined and used to coregister the slave to the master image. Using the master and coregistered slave image the interferometric phase is computed as the complex conjugated product of the two complex images.

The last two steps are the computation of the ellipsoid phase ("flat Earth") and the topographic phase. The flat Earth phase is approximated using the precise orbits, by a 2D-polynomial of degree 5 and the topographic phase is computed using the precise orbits and the digital terrain model SingDTM. The final result was geolocated to the WGS84/GRS80 map geometry.

A first analysis of the 21 interferograms revealed a low coherence for interferograms with perpendicular baseline greater than 400m and a good coherence on the urban areas (a significant percentage of the total area of Singapore) for temporal baselines up to 360 days. On urban areas, the limiting factor is clearly the perpendicular baseline. On coherent interferograms, it was identified the presence of significant tropospheric noise and no evidence of large deformation signal.

4. PERSISTENT SCATERERS PROCESSING

The aim of Persistent Scatterer technique is to overcome interferometric coherence degradation over time using a set of phase-stable pixels (the persistent scatterers) [9], [10]. Basically it works by examining a stack of differential interferograms and looking at the temporal evolution of phase-stable pixels. Because this technique needs phase-stable (persistent) pixels it is especially good for use over urban areas, where temporal decorrelation effects are minimized due to the high number of stable reflective structures (buildings, bridges, etc). STAMPS software [10] was used in the Persistent Scatterers processing.

The preliminary estimation is limited to a coarse set of pixels, the Persistent Scatterers Candidates, PSC, used on a preliminary estimation of the atmospheric phase at these pixels in all interferograms. The PSC were selected using the amplitude dispersion index and a PSC is selected if the amplitude dispersion index is below

0.4.

The estimated height of the persistent scatters is a good indicator of the overall result quality. Gross errors on the estimated height are possibly associated with gross errors on other estimated quantities (velocity, atmosphere). The estimated heights for ascending and descending passes were compared with the digital terrain model. A standard deviation of 3 m of the height residuals was found, with a minimum and maximum error of -46m and 32m, respectively. Persistent Scatters with residuals higher than 6m (2σ) were eliminated.

The resulting ascending and descending data sets are 20178 and 59905 PSs, respectively.

5. RESULTS AND DISCUSSION

5.1 Integration INSAR / GPS Data

Ascending and descending passes estimated velocities are not directly comparable due to different observation angles. In fact, the estimated result is the line of sight (LOS) velocity, which is dependent on the acquisition geometry. In order to convert line of sight velocity to vertical velocity the geometry of the acquisition and the horizontal velocity must be known. The geometry of acquisition is known and the horizontal velocity can be given by GPS stations. The strategy used to convert LOS velocities into vertical velocities is based on the combination of sparse GPS 3D-velocities with two sets of Persistent Scatterers determined from ascending and descending passes, see [4].

The input data are: a set of GPS - 3D velocities relative to ITRF2008 (Figure 1) and two sets of Persistent Scatterers corresponding to the descending and ascending orbits. Although the time period for the InSAR and GPS observations are different: 1995-2000 and 2006-2012, respectively. Initially, the horizontal components of the velocity (East and North) are assigned to each PS from interpolation of available GPS observations. Then, the vertical component of the velocity is determined, for each PS, from the LOS velocity and the horizontal components of the velocity. Latter the vertical offsets are numerically determined by comparison between GPS (ITRF velocities) and the two sets of PS (ascending and descending). These values are then used to create the vertical deformation map of Singapore with considerably better resolution and accuracy than each single set of observations (SAR and GPS). We have assumed there are no active faults or significant relative horizontal deformation in Singapore in this period.

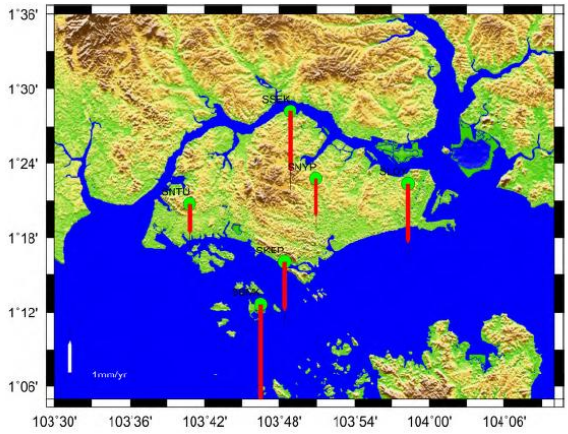

Figure 1. Vertical velocity computed from GPS data in the period 2007 / 2010.(adapted from [11])

PS's from ascending and descending tracks were analysed separately. PS's vertical velocities are compared with GPS estimated velocities selecting all PS's in a circle of 100m centred on the GPS station. The results, after combination of GPS and INSAR velocities, are presented in Tab. 2.

Table 2. Differences between GPS vertical velocities and PS's vertical velocities (all values are mm/yr)

GPS station	GPS vertical velocity	Residuals descending		Residuals ascending	
		mean	std	mean	std
SSEK	-2.0 +- 1.3	-0.29	1.2	-0.09	1.2
SNTU	-1.0 +- 1.1	0.88	0.8	0.97	1.0
SLOY	-1.9 +- 0.9	0.12	1.3	0.00	1.2
SNYP	-1.3 +- 0.9	0.21	0.8	0.07	1.2
SKEP	-1.6 +-1.0	-1.48	0.7	-0.83	1.2

InSAR estimated velocity is inherently slant and relative. The merging process has projected slant velocities into vertical velocities and has unbiased the velocities geo-referencing them to ITRF2008 (the reference system used for GPS processing). For both tracks, mean residuals are close to zero. The only exception is SKEP station where the mean residual is higher than the signal. For descending pass, the residuals standard deviation is within 1sigma GPS velocities. On the contrary, for ascending pass the error is greater than 1σ in all stations.

The resulting integrated vertical land deformation is depicted in Fig. 2.

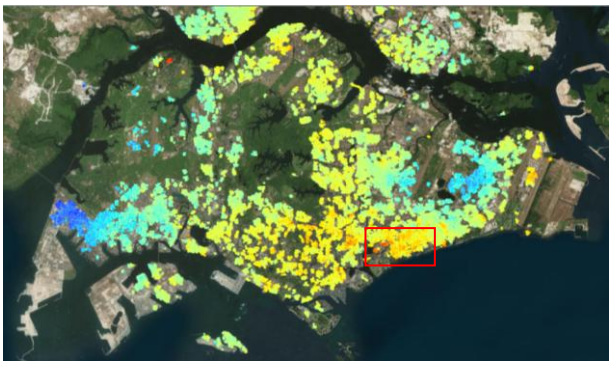

Figure 2. Vertical land deformation in the period 1995-2000. Linear rainbow colour scale from -9 mm (red) to 5mm/yr (blue). Red rectangle is discussed in Figures 3 and 4.

5.2 Comparison with ground levelling

On Singapore there is a network of levelling lines covering all territory that were last measured in 2010. For some few marks it was possible to assess previous measurements made in 1998. These marks are shown in Fig. 3 as squares. To compare the levelling with PS velocities we draw a line connecting some of these marks and compute the displacement rate profile. The subsidence rate along the profile was computed averaging the velocities of all PS within a distance of 100 m. The connecting line is shown in Fig. 3 and the profile in Fig. 4.

Unfortunately the acquisition time of the images (1995-2000) do not overlap the levelling period (1998-2010). Even then, the levelling results have a high degree of agreement with the computed INSAR displacement rates. Assuming an error of 4mm/yr (phase error 30°) for the INSAR results we see that all but one benchmarks are within the error. However, there are some discrepancies not shown in the profile but seen in Fig.3. There are two red benchmarks on the top left with a displacement rate of -10 mm/yr that are in complete disagreement with closer PSs. This is probably due to a local subsidence phenomena occurred after the last image acquisition in 2000.

Figure 3. Vertical land deformation in Marine Parade area (red rectangle on Figure 2). Levelling marks (coloured squares) and profile in red.

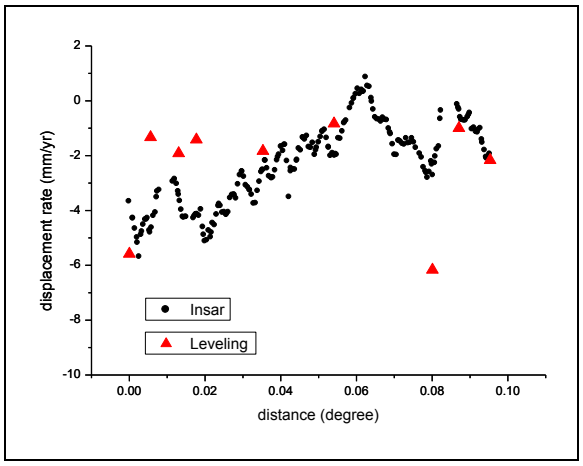

Figure 4. InSAR profile and levelling marks displacement rate (mm/yr).

5.3 Spatial Analysis of deformation

The resulting PSs vertical velocities were integrated in a GIS environment allowing combining interactively deformation measurements with other geographic, geophysical and geological data (cf. Fig. 2). This may facilitate reliable risk assessment and control of hazardous areas, including time/space monitoring of vertical land movement as well as precise stability checking of single buildings and infrastructures.

The vertical deformation, from 1995 to 2000, has a mean value of -1.5 mm/yr and a standard deviation of 1.7 mm/yr. The overall area is subsiding especially on the perimeter of Singapore while some areas are uplifting perhaps due to local site disturbances. The subsidence rate is higher near the sea decreasing with the distance to the shore. Critical areas are the Business district and the Marine Parade areas to with relatively high values of subsidence and height above 5 m. For Marine Parade area (signalized in Fig. 1), the vertical deformation is also shown in Fig 4. The subsidence rate ranges from -4 to -7 mm/yr.

The result seems to be reliable and consistent with the geologic setting pointing the scatter pattern of deformation to artificial causes. Other examples of subsidence due to anthropogenic interventions are: Bangkok [3], Hong Kong [5], Mexico City [12], Paris [13] or Lisbon [4]. Most are due to ground water exploration, built structures or reclaimed areas that involve the settlement of the ground surface and affect wide areas.

6. CONCLUSIONS

The Persistent Scatteers technique was applied to a set of ascending and descending ERS1&2 SAR data to detect and characterize the subsidence in Singapore. It was verified that Singapore mainland has experienced a subsidence phenomena from 1995 to 2000 with a mean subsidence rate of -1.5 mm/yr, which is detected consistently by combined InSAR and GPS analysis. On some localized areas, a significant subsidence with subsiding rates of -7 mm/yr was detected. Highest subsiding rates are near the shore on low flat land, above 5m. The result seems to be reliable and consistent with the geologic setting. The scatter pattern of the deformation indicates anthropogenic causes related with consolidation of built and/or reclaimed areas, rather than a natural causes.

7. REFERENCES

1. P. Tkalich P. Vethamony Q.-H. Luu and M. T. Babu, 2013. Sea level trend and variability in the Singapore Strait, Ocean Sci., 9, 293-300, 2013.
2. Raju, D.K., K. Santosh, J. Chandrasekar and Teh Tiong-Sa, 2010. Coastline change measurement and generating risk map for the coast using Geographic Information System, The International Archives of the Photogrammetry, Remote Sensing and Spatial Information Sciences, Vol. 38, Part II
3. Aobpaet, A., Cuenca, M.C., Hooper, A. et al., 2009. Land subsidence evaluation using InSAR time series analysis in Bangkok metropolitan area. In Proceeding of FRINGE09 workshop, Frascati, Italy, 7p. 30 November–4 December 2009.
4. Catalão, J., G. Nico, R. Hanssen, C. Catita, 2010. Merging GPS and atmospherically corrected InSAR data to map 3D terrain displacement velocity. IEEE Transactions on Geoscience and Remote Sensing, Volume: 49, Issue: 6, Part: 2, doi:10.1109/TGRS.2010.2091963.
5. Chen, Q., G. Liu, X. Ding, J-C Hu, L. Yuan, P. Zhong, M. Omura, 2010. Tight integration of GPS observations and persistent scatterer InSAR for detecting vertical ground motion in Hong Kong. International Journal of Applied Earth Observation and Geoinformation 12 (2010) 477–486
6. Ferretti, A., Monti-Guarnieri, A., Prati, C., Rocca, F., Massonnet, D., 2007. InSAR Principles: Guidelines for SAR Interferometry Processing and Interpretation. ESA Publications TM-19, ESTEC, Editor: Karen Fletcher.
7. Colesanti, C., A. Ferretti, C. Prati and F. Rocca, 2003. Monitoring landslides and tectonic motions with the permanent scaterers technique, Eng. Geol, 68 (1-2), 3-14.
8. Kampes, B., R. Hanssen., Z. Perski, Radar Interferometry with Public Domain Tools, Proceedings of FRINGE 2003, December 1-5, Frascati, Italy, 2003.
9. Ferretti, A., Prati, C. Roca, F., 2001.Permanent Scatterers in SAR inyerferometry. IEEE Trans. Geosci. Remote Sensing 39 (1), 8-20.
10. Hooper, A., P. Segall, H. Zebker, Persistent scatterer interferometric synthetic aperture radar for crustal deformation analysis, with application to Volcano Alcedo, Galapagos, Journal of Geophysical Research-Solid Earth, 112(B7), B07407, 2007.
11. Fernandes, R. M. S., Raju, D., and Khoo, V.: Evaluation of the Tectonic Stability of Singapore based on SiReNT, Joint International Symposium on Deformation Monitoring, Hong Kong, Nov 4, 2011.
12. Osmanoglu, B., T.H. Dixon, S. Wdowinski, E. Cabral-Cano, Y. Jiang, Mexico City Subsidence Observed with Persistent Scatterer InSAR (2011), Journal of Applied Earth Observation and Geoinformation, 13(1), 1-12, 2011, doi:10.1016/j.jag.2010.05.009.
13. Fruneau, B., F. Sarti, “Detection of ground subsidence in the city of Paris using radar interferometry: isolation of deformation from atmospheric artifacts using correlation”, Geophysical Research Letters, Vol. 27, No. 24, 2000, pp. 3981-3984.